Journal of Biomechanics 43 (2010) 2771–2779

Contents lists available at ScienceDirect

Journal of Biomechanics

journal homepage: www.elsevier.com/locate/jbiomech
www.JBiomech.com

The influence of altering push force effectiveness on upper extremity demand during wheelchair propulsion

Jeffery W. Rankin [a], Andrew M. Kwarciak [b], W. Mark Richter [b], Richard R. Neptune [a,*]

[a] Department of Mechanical Engineering, The University of Texas at Austin, 1 University Station C2200, Austin, TX 78712, USA
[b] MAX Mobility, LLC, Antioch, TN, USA

ARTICLE INFO

Article history:
Accepted 3 June 2010

Keywords:
Forward dynamics simulation
Push technique
Musculoskeletal model
Handrim force
Biomechanics

ABSTRACT

Manual wheelchair propulsion has been linked to a high incidence of overuse injury and pain in the upper extremity, which may be caused by the high load requirements and low mechanical efficiency of the task. Previous studies have suggested that poor mechanical efficiency may be due to a low effective handrim force (i.e. applied force that is not directed tangential to the handrim). As a result, studies attempting to reduce upper extremity demand have used various measures of force effectiveness (e.g., fraction effective force, FEF) as a guide for modifying propulsion technique, developing rehabilitation programs and configuring wheelchairs. However, the relationship between FEF and upper extremity demand is not well understood. The purpose of this study was to use forward dynamics simulations of wheelchair propulsion to determine the influence of FEF on upper extremity demand by quantifying individual muscle stress, work and handrim force contributions at different values of FEF. Simulations maximizing and minimizing FEF resulted in higher average muscle stresses (23% and 112%) and total muscle work (28% and 71%) compared to a nominal FEF simulation. The maximal FEF simulation also shifted muscle use from muscles crossing the elbow to those at the shoulder (e.g., rotator cuff muscles), placing greater demand on shoulder muscles during propulsion. The optimal FEF value appears to represent a balance between increasing push force effectiveness to increase mechanical efficiency and minimize upper extremity demand. Thus, care should be taken in using force effectiveness as a metric to reduce upper extremity demand.

1. Introduction

Up to 70% of manual wheelchair users will develop upper extremity (UE) overuse injuries and/or pain (Finley and Rodgers, 2004). This high incidence is associated with the high load requirements and low mechanical efficiency (i.e. ratio of external work to metabolic cost) involved in wheelchair propulsion, which places considerable physical demand on the UE (e.g., Finley et al., 2004; Mercer et al., 2006). One possible reason for the low mechanical efficiency (de Groot et al., 2004; Veeger et al., 1991) is that users generate non-tangential handrim forces that do not contribute to accelerating the wheelchair forward (e.g., Boninger et al., 1997), resulting in ineffective use of generated muscle force. To quantify force effectiveness during a push, previous studies have used the ratio of tangential to total handrim force (i.e. fraction of effective force, FEF) and found average FEF values between 0.26 and 0.81 (1.0 indicates an entirely tangential force) (Boninger et al., 1999; Dallmeijer et al., 1998; Lin et al., 2009). Thus, redirecting the handrim force more tangentially may improve mechanical efficiency and reduce overall UE demand. As a result, studies have used FEF to help develop training programs (e.g., de Groot et al., 2002a; Kotajarvi et al., 2006), as a guide to modify wheelchair configuration (e.g., Aissaoui et al., 2002; Guo et al., 2006) and to compare propulsion techniques (e.g., Boninger et al., 2002; Goosey-Tolfrey et al., 2006).

However, studies attempting to relate FEF to UE demand have found mixed results. Dallmeijer et al. (1998) found that tetraplegic wheelchair users had lower mean FEF and mechanical efficiency values compared to paraplegic users at low and moderate propulsion intensities, suggesting that increased FEF reduces UE demand. In contrast, de Groot et al. (2002b) found that non-wheelchair users who received FEF feedback increased mean FEF but reduced mechanical efficiency compared to a control group, suggesting that increasing FEF also increases UE demand. Others found no correlation between FEF and peak shoulder strength in experienced wheelchair users (Ambrosio et al., 2005). The different results across studies may be due to the challenge of relating FEF to UE demand.

Modeling studies seeking to understand the relationship between FEF and UE demand have found that high FEF values

* Corresponding author. Tel.: +512 471 0848; fax: +512 471 8727.
E-mail address: rneptune@mail.utexas.edu (R.R. Neptune).

0021-9290/$ - see front matter © 2010 Elsevier Ltd. All rights reserved.
doi:10.1016/j.jbiomech.2010.06.020

increase net shoulder moments in young (Bregman et al., 2008) and elderly (Desroches et al., 2008a, 2008b) subjects, increase joint- (Rozendaal et al., 2003) and muscle-based (Bregman et al., 2008) cost functions and glenohumeral constraint force requirements (Bregman et al., 2008). Bregman et al. (2008) also related UE demand to increases in FEF using muscle work and power estimates obtained from net joint moments. However, no study has quantified individual muscle contributions to the handrim forces or related bidirectional changes in FEF to individual muscle work, power and stress quantities, which can provide additional insight into how changing FEF influences muscle recruitment. The purpose of this study was to build upon these previous studies by developing a forward dynamics simulation of the push phase of wheelchair propulsion to understand the relationship between FEF and UE demand by determining how changing FEF affects individual muscle contributions to the tangential handrim force and their corresponding muscle work and stress values.

2. Methods

2.1. Musculoskeletal model

An upper extremity musculoskeletal model was developed using SIMM (Musculographics, Inc.) based on the work of Holzbaur et al. (2005). The model consisted of rigid bodies representing the trunk and right upper arm, forearm and hand, with mass and inertia characteristics determined using anthropometric regression equations (Clauser et al., 1969) (Fig. 1). The model had six rotational degrees of freedom representing trunk lean and shoulder, elbow and forearm articulations. Scapular and clavicular motions were prescribed as a function of shoulder elevation (de Groot and Brand, 2001). Trunk lean was prescribed based on experimental data and hand translations were constrained to follow the circular handrim path. Passive torques representing forces applied by ligaments and other passive joint structures were applied at the shoulder and elbow to limit extreme joint angles using equations similar to those developed for the lower limb (Davy and Audu, 1987). The dynamic equations of motion were generated using SD/FAST (Parametric Technology Corp.).

Twenty-six Hill-type musculotendon actuators with parameters derived from Holzbaur et al. (2005) and governed by intrinsic muscle force–length–velocity relationships (Zajac, 1989) were used to represent the major UE muscles crossing the shoulder and elbow joints. Musculotendon lengths and moment arms were fit with polynomial equations (Menegaldo et al., 2004) over the complete range of motion for each joint during wheelchair propulsion. The order of each polynomial equation was increased until fit errors during the simulations were either less than 10% of the corresponding maximal value of the musculotendon length (moment arm) or 3 mm, whichever was greater. Actuators were combined into sixteen muscle groups based on similar anatomical classification and electromyographic (EMG) data, with muscles within each group receiving the same excitation signal (Fig. 1, Table 1). When EMG data were not available or limited, independent excitation patterns were used. Muscle excitation–activation dynamics were modeled using a first order differential equation (Raasch et al., 1997) with muscle specific activation and deactivation time constants (Happee and Van der Helm, 1995; Winters and Stark, 1988).

2.2. Dynamic optimization

A global optimization algorithm (simulated annealing, Goffe et al., 1994) was used to perform three optimizations. First, a nominal forward dynamics simulation of the push phase of a representative wheelchair user was generated using the optimization algorithm with an optimal tracking cost function (Neptune et al., 2001) to identify the muscle excitation patterns that minimized the difference between simulation and experimentally measured push phase data (see experimental data below). Cost function quantities included UE joint kinematics and three-dimensional handrim forces. Two additional optimizations were performed that maximized and minimized FEF over the push phase while minimizing differences between the experimental joint kinematics and tangential handrim force.

Neural excitation patterns were defined using the linear sum of two parameterized Henning patterns, which required six excitation parameters (two magnitudes, onset and offset values) for each muscle group, resulting in a total of ninety-six parameters to be optimized. The excitation timing parameters for muscle groups with EMG data available were constrained to correspond with the experimental data. Timing parameters for groups without EMG data were left unconstrained.

2.3. Experimental data

Experimental data were collected from a representative manual wheelchair user who was a 36 year old male with paraplegia (T12) and had over 13 years of wheelchair experience. The subject's height and weight were 177.8 cm and 80.7 kg, respectively. Prior to data collection, the subject provided informed consent. All data collection procedures were performed at MAX Mobility, LLC (Antioch, TN).

Testing was conducted on a custom-built wheelchair treadmill while the subject propelled his own wheelchair at his self-selected speed of 0.84 m/s and cadence of 51.1 pushes/minute. Shoulder and elbow kinematics were obtained using a 3-camera motion capture system (Phoenix Technologies) and an active marker set (Fig. 2). Marker data were collected at 100 Hz and low-pass filtered (10 Hz) using an eighth-order Butterworth filter. Handrim kinetics and wheel angle were recorded at 200 Hz using an OptiPush force sensing wheel (MAX

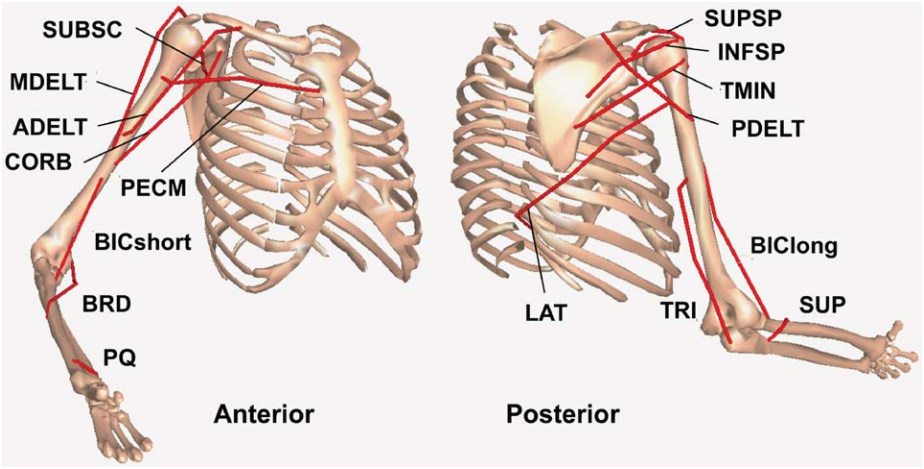

Fig. 1. Musculoskeletal model used in the wheelchair propulsion simulations. The model had 6 degrees of freedom consisting of trunk lean, shoulder elevation plane, shoulder elevation angle (thoracohumeral angle), shoulder internal–external rotation, elbow flexion-extension and forearm rotation (pronation-supination). The 16 muscle groups used to drive the model were: anterior deltoid (ADELT), middle deltoid (MDELT), posterior deltoid (PDELT), pectoralis major clavicular and sternal heads (PECM), 3 part latissimus dorsi and teres major (LAT), subscapularis (SUBSC), infraspinatus (INFSP), teres minor (TMIN), supraspinatus (SUPSP), brachialis and short head of the biceps brachii (BICshort), coracobrachialis (CORB), long head of the biceps brachii (BIClong), combined anconeous and lateral, medial and long heads of the triceps brachii (TRI), supinator (SUP), pronator quadratus (PQ) and combied pronator teres, and brachioradialis (PT).

Table 1
Upper extremity muscle parameters.

Muscle	Peak isometric force (N)	Optimal fiber length (m)	Tendon slack length (m)	Pennation angle (deg)
ADELT group				
Anterior deltoid	1142.6	0.12	0.123	22
MDELT group				
Middle deltoid	1142.6	0.1078	0.1095	15
PDELT group				
Posterior deltoid	259.88	0.1367	0.038	18
PECM group				
Pectoralis major, clavicular head	364.41	0.1242	0.0228	17
Pectoralis major, sternal head 1	515.41	0.1385	0.089	25
Pectoralis major, sternal head 2	390.55	0.1385	0.152	25
LAT group				
Teres major	425.39	0.1624	0.02	16
Lattissimus dorsi 1	389.1	0.254	0.12	25
Lattissimus dorsi 2	389.1	0.2324	0.1765	19
Lattissimus dorsi 3	281.66	0.2789	0.1403	21
SUBSC group				
Subscapularis	1377.81	0.0873	0.033	20
INFSP group				
Infraspinatus	1210.84	0.0805	0.05	18.5
TMIN group				
Teres Minor	354.25	0.0741	0.0813	24
SUPSP group				
Supraspinatus	487.82	0.0682	0.0595	7
BICshort group				
Brachialis	987.26	0.0858	0.065	0
Bicepts brachii, short head	435.56	0.1321	0.2123	0
CORB group				
Coracobrachialis	242.46	0.0932	0.097	0
BIClong group				
Biceps brachii, long head	624.3	0.1557	0.3	0
TRI group				
Anconeous	350	0.027	0.018	0
Triceps brachii, lateral	624.3	0.1138	0.098	9
Triceps brachii, medial	624.3	0.1138	0.0908	9
Triceps brachii, long head	798.52	0.134	0.217	12
SUP group				
Supinator	476	0.033	0.028	0
PQ group				
Pronator quadratus	75.48	0.0282	0.005	10
BRD group				
Pronator teres	566.22	0.0492	0.098	10
Brachioradialis	261.33	0.1726	0.133	0

Mobility, LLC; Richter and Axelson, 2005) and low-pass filtered (20 Hz) using an eighth-order Butterworth filter. Raw EMG data were collected from the anterior, middle and posterior portions of the deltoid, sternal portion of the pectoralis major, biceps brachii and medial and lateral portions of the triceps brachii (Fig. 2) at 1500 Hz using surface electrodes and then rectified, band-pass filtered (10–500 Hz) and smoothed using a 100 ms moving average window.

Data were collected for 10 complete strokes, with stroke limits defined by kinetic data from the wheel. Each stroke began when a discernible radial or tangential force was applied to the handrim and ended at the start of the following stroke. The end of the push phase was defined as the time when handrim forces returned to the baseline value. Data for each stroke were normalized to 100% of the stroke using cubic spline interpolation and averaged over all strokes to create representative biomechanical and muscle excitation profiles.

2.4. Analysis

Three consecutive propulsion cycles were simulated for each optimization and data were analyzed during the third push phase to assure that the simulation reached steady-state. For each simulation, minimum, maximum and average FEF values were determined. Individual muscle contributions to the handrim forces and how these contributions changed with FEF were determined by independently applying each muscle force to the model and calculating the resultant handrim forces. The push phase was divided into three equal regions that approximate regions of (1) increasing, (2) peak and (3) decreasing upper extremity power (Price et al., 2007) and average muscle contributions were determined within each region. To determine if the resulting simulation muscle activity was consistent with each muscle's capacity to contribute to the handrim forces, an additional analysis was performed that calculated each muscle's average contribution to the handrim forces during each region when applying a constant muscle force of 100 N.

To assess the influence of FEF on upper extremity demand, muscle stress was calculated as the percentage of maximum isometric force generated by each muscle at every time step and average and maximum values were determined. Total, positive and negative muscle work were quantified by integrating the positive and negative musculotendon power.

3. Results

All simulations replicated well the experimental joint kinematics and handrim tangential force (Fig. 3) with average errors of 1.12° and 2.36 N, respectively. The simulations also produced different average FEF values, with the nominal, maximal and minimal FEF simulations having values of 0.61, 0.80 and 0.30, respectively. The maximal FEF simulation produced an entirely tangential force (i.e. FEF > 0.99) for 29% of the push (region: 41–70% push phase), while peak FEF for the minimal FEF simulation was 0.45. The nominal simulation followed the experimental FEF values over the push, peaking at 0.87.

All three simulations had a small initial region (3–5% of the push phase) where FEF did not surpass 0.10.

The average stress across all muscles was lowest for the nominal FEF simulation (9.2% versus 11.3% and 19.5% for the maximal and minimal simulations). Anterior deltoid (ADELT), posterior deltoid (PDELT), pronator quadratus (PQ) and subscapularus (SUBSC) consistently had higher stress values, surpassing 12% in all three simulations (Fig. 4(A)). Infraspinatus (INFSP) and teres minor (TMIN) had high average stress values in the maximal and minimal FEF simulations ($>13\%$). Peak stresses exceeded 40% for many of these muscles, with some stress values surpassing 100% due to active stretching (Fig. 4(B)).

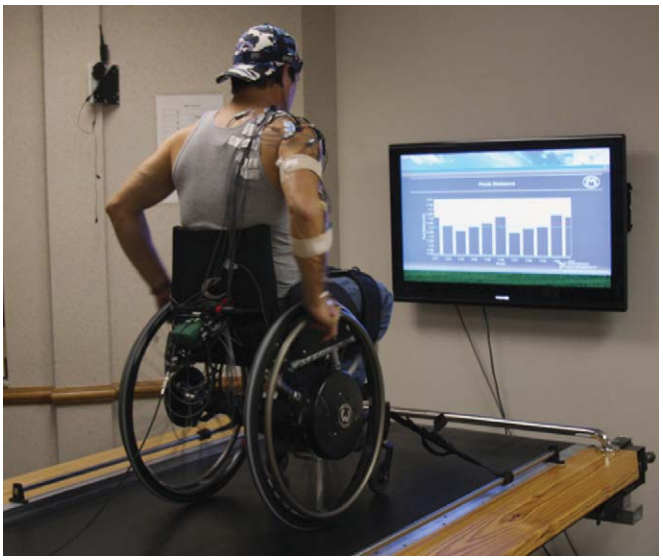

Fig. 2. Experimental setup used to collect upper extremity kinematics, handrim forces and muscle EMG during wheelchair propulsion on a treadmill. Active markers were placed on the head and sternum, and on the right acromium process, lateral epicondyle, radial and ulnar styloids, third and fifth metacarpophalangeal joints, second proximal interphalangeal joint and wheelchair hub to collect kinematic data. An OptiPush instrumented wheel (MAX Mobility, Antioch, TN) was used to measure forces between the wheel and the chair axle. EMG data were collected via surface electrodes from the anterior, middle and posterior portions of the deltoid, sternal portion of the pectoralis major, biceps brachii and medial and lateral portions of the triceps brachii.

Total muscle work was lowest in the nominal simulation, with muscle work increasing by 28% and 71% in the maximal and minimal FEF simulations, respectively. The increased work was due primarily to additional positive work generated by INFSP and negative work generated by PDELT and middle deltoid (MDELT) (Fig. 5). There was also increased positive work generated by pectoralis major (PECM) in the maximal FEF simulation and SUBSC in the minimal FEF simulation (Fig. 5). The triceps group (TRI) increased positive and negative work when minimizing FEF, but reduced total work when maximizing FEF (Fig. 5).

Muscle contributions to the handrim forces during the simulations were consistent with their capacity with the exception of MDELT, which can generate tangential force during region 1 but was not utilized (Figs. 6 and 7). For all simulations, the biceps group (combined BICshort and BIClong, BIC) and brachioradialis (BRD) had the highest average contributions to the tangential force during region 1 and TRI and ADELT during regions 2 and 3 (Fig. 6). Muscles contributing most to the radial force were ADELT during regions 1 and 2, MDELT during region 3 and TRI over all regions (Fig. 7). Muscle contributions to the handrim forces changed with FEF. The maximal FEF simulation increased tangential force contributions from BRD during region 1 and PECM, CORB and INFSP during region 2 (Fig. 6). BRD and INFSP had larger negative contributions to the radial force during regions 1 and 3, respectively, while PECM and CORB increased their radial force contributions during region 2. In the minimal FEF simulation, BRD reduced and SUBSC increased their

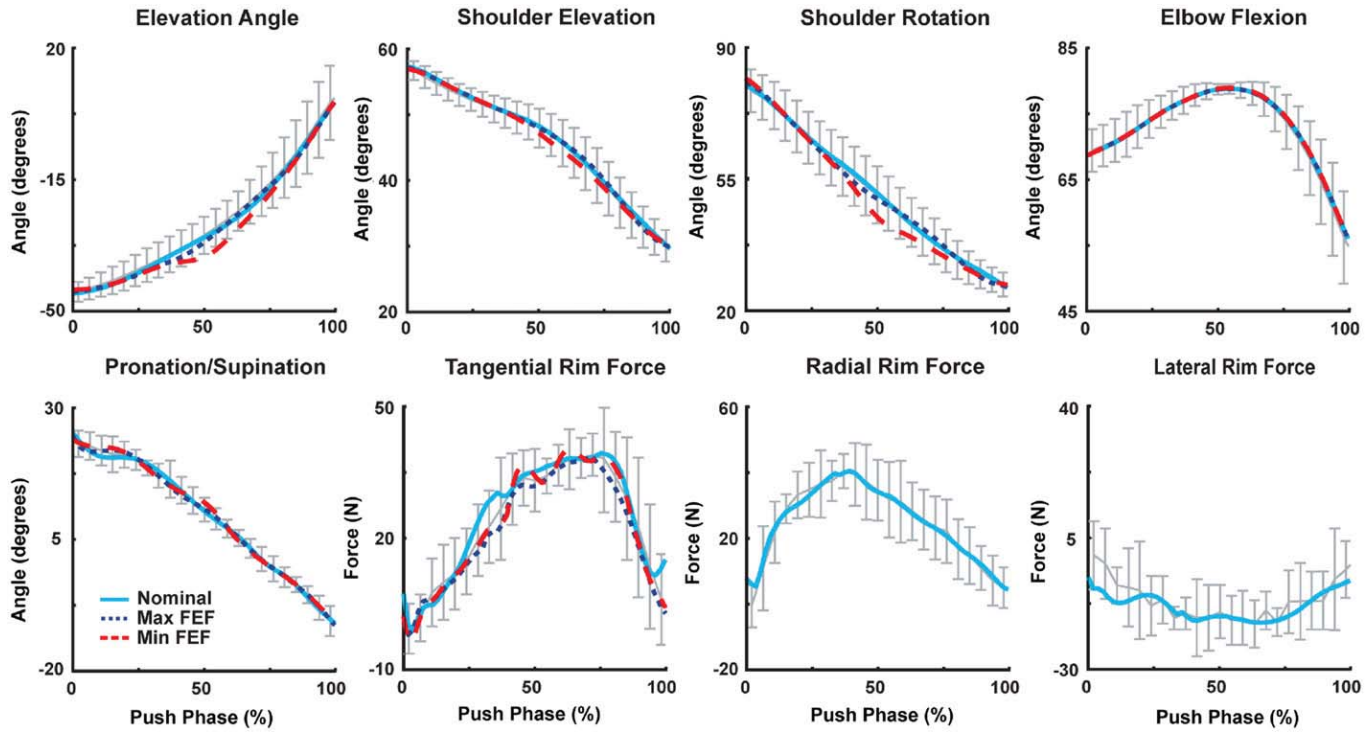

Fig. 3. Comparisons between the experimental kinematics and handrim kinetics (bars indicate ± 2SD) and the nominal (solid), maximal FEF (dotted) and minimal FEF (dashed) simulations. The radial and lateral rim forces were not tracked in the maximal and minimal FEF simulations; instead the optimization modified these forces to change the average FEF over the push.

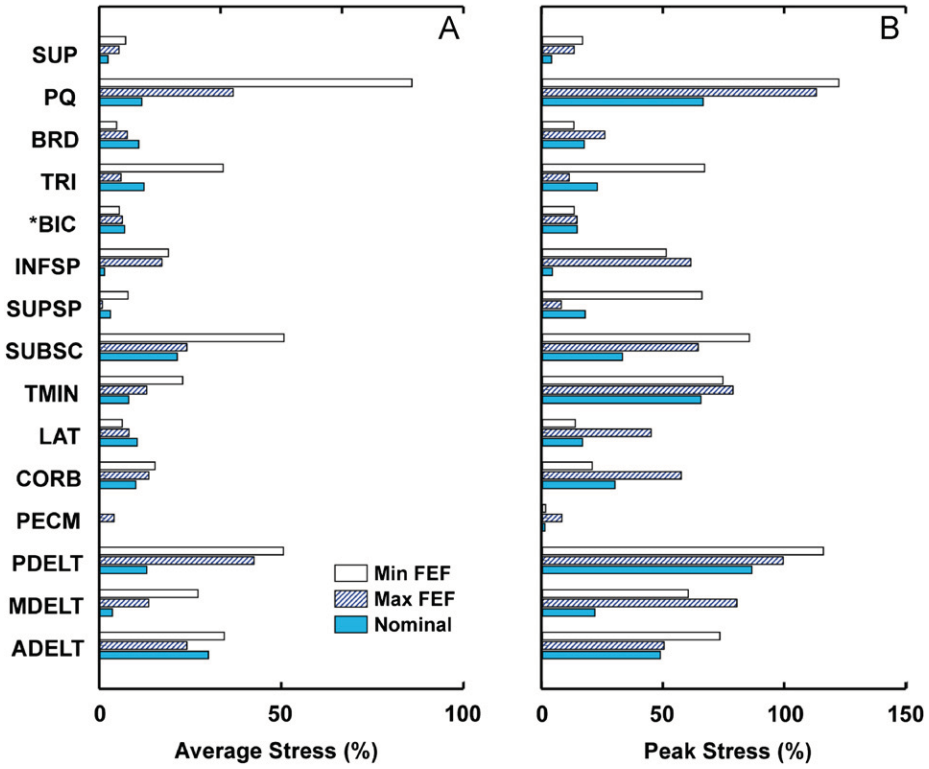

Fig. 4. Muscle stress for each muscle group in the model. (A) Average stress over the entire push and (B) peak stress. Peak stress values were higher than 100% at times due to active stretching of some muscles during the push. *BICshort and BIClong are combined into BIC.

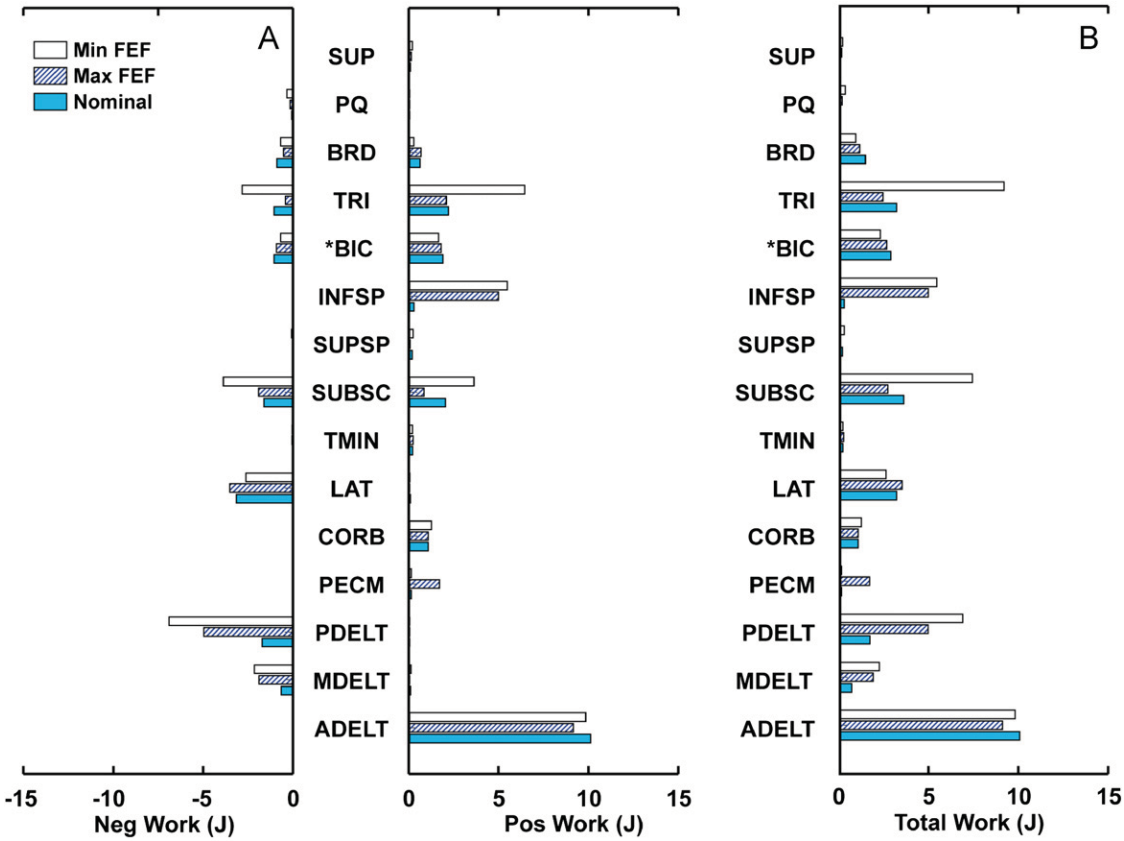

Fig. 5. Individual muscle group work over the entire push phase for each simulation. (A) Muscle group positive and negative work and (B) total work (absolute value summation of positive and negative work). *BICshort and BIClong are combined into BIC.

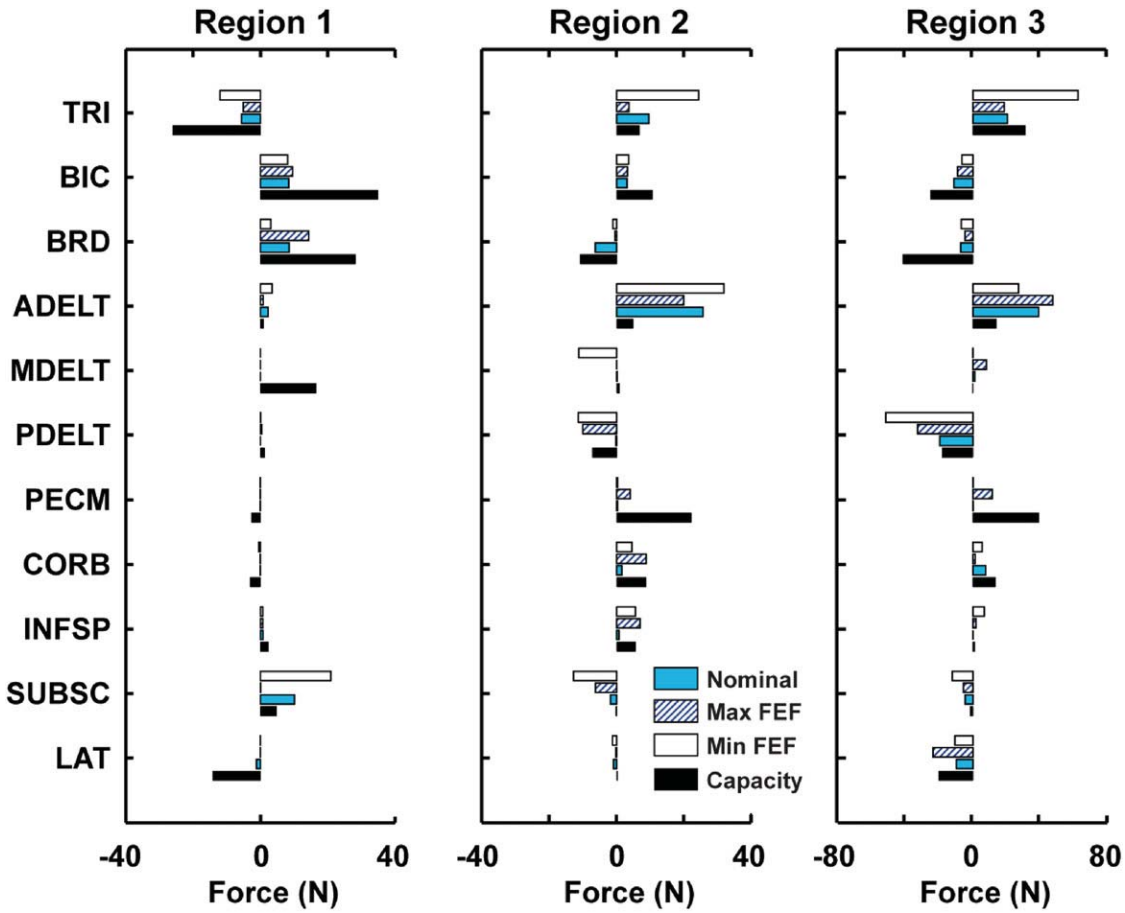

Fig. 6. Average muscle force contributions to the tangential force from the primary muscle groups used during the three regions of the push phase. A positive contribution indicates a propulsive force on the handrim. Capacity (black) represents the average force contributions if each muscle were to generate a constant 100 N force over the entire push. All other muscle groups had minimal ability to affect the handrim forces.

contributions to the positive tangential force during region 1 (Fig. 6). During regions 2 and 3, TRI increased positive contributions and MDELT and PDELT increased negative contributions to the tangential force (Fig. 6). TRI also increased its positive contributions to the radial force during all regions in the minimal FEF simulation (Fig. 7). All other muscle groups had minimal ability to influence the handrim forces.

4. Discussion

Comparisons between the three simulations revealed that FEF strongly influences muscle work and stress and overall UE demand during wheelchair propulsion. While the tangential force was maintained in all three simulations to generate the required wheelchair speed, the maximal and minimal FEF simulations greatly altered the lateral and radial forces, which resulted in increases in the total muscle work. Maximizing FEF increased muscle work primarily through increased work by the shoulder muscles, with additional positive work generated by INFSP and PECM and increased negative work generated by MDELT and PDELT (Fig. 5). The work generated by the elbow muscles decreased, primarily through reduced TRI negative work (Fig. 5). These results are consistent with the previous studies that showed higher FEF values increased shoulder moments (Desroches et al., 2008a, 2008b) and rotator cuff muscle power generation (Bregman et al., 2008). In the minimal FEF simulation, INFSP, SUBSC and TRI increased positive muscle work while MDELT, PDELT and TRI increased negative work (Fig. 5), suggesting that minimizing FEF increases muscle co-contraction.

In all simulations, there were multiple muscles with high average stresses, supporting the notion that wheelchair propulsion exerts a high physical demand on the UE. Peak stresses for PQ, TMIN, SUBSC, ADELT and PDELT were greater than 40% in all three simulations, with average stresses exceeding 25% in many cases (Fig. 4). These results are consistent with previous studies showing high recruitment of ADELT and PDELT (e.g., Mulroy et al., 2004) and others predicting high SUBSC, PQ, ADELT and PDELT forces during nominal wheelchair propulsion (Lin et al., 2004; van Drongelen et al., 2005; Veeger et al., 2002). Although none of these studies showed a high TMIN force, there were high forces in other rotator cuff muscles (e.g., INFSP) not present in the nominal simulation of this study. This suggests that TMIN may replace the functions performed by other rotator cuff muscles in previous studies. Both maximizing and minimizing FEF increased average stress in these muscles, with the exception of ADELT, which only increased when minimizing FEF. In addition, altering FEF greatly increased INFSP stress from less than 5% in the nominal simulation to almost 20% when FEF was minimized. Previous studies have shown high forces in this muscle (Lin et al., 2004; Veeger et al., 2002), suggesting that INFSP may play an important role in propulsion. The high stress in the rotator cuff muscles (SUBSC, TMIN and INFSP) during the push phase may explain the high prevalence of rotator cuff injuries and pain in wheelchair users.

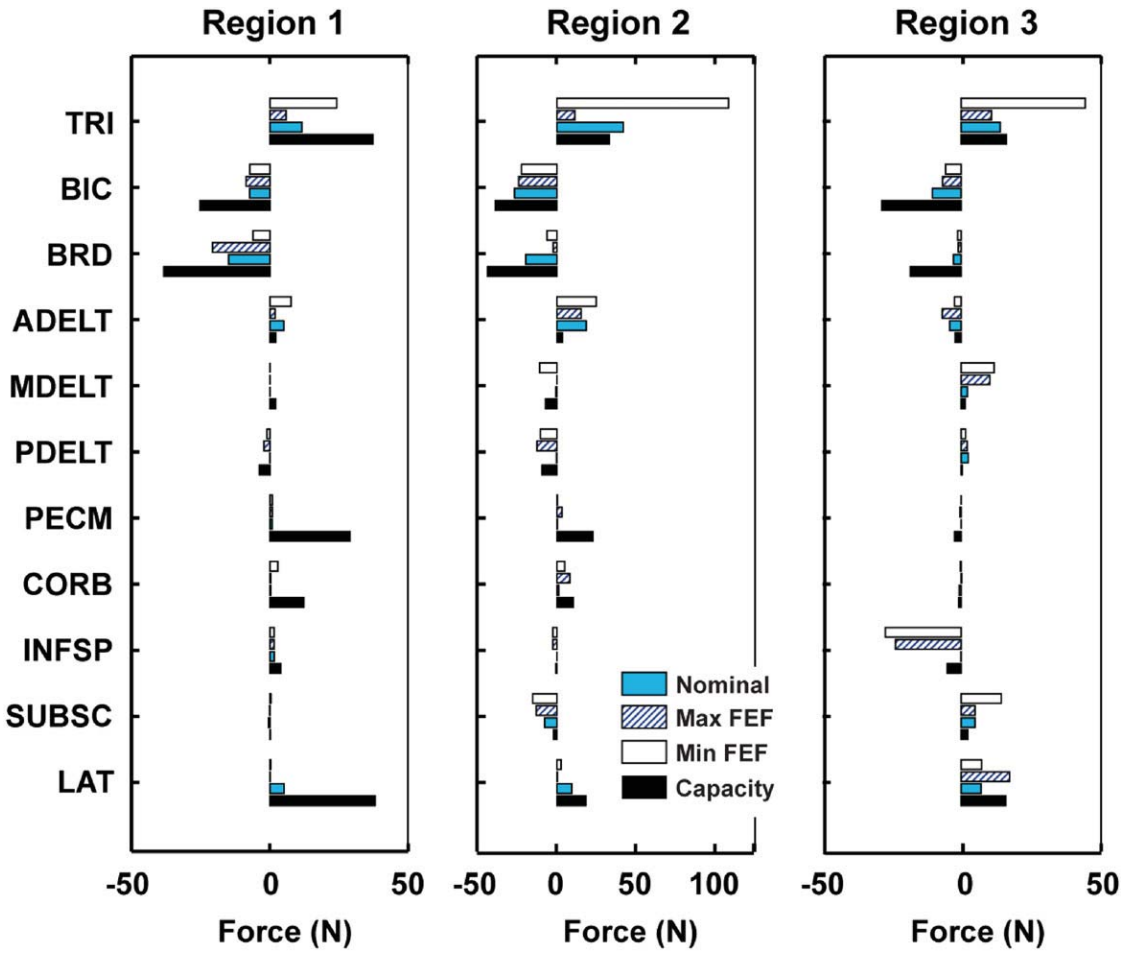

Fig. 7. Average muscle force contributions to the radial force from the primary muscle groups used during the three regions of the push phase. A positive contribution indicates a compressive force on the handrim. Capacity (black) represents the average force contributions if each muscle were to generate a constant 100 N force over the entire push. All other muscle groups had minimal ability to affect the handrim forces.

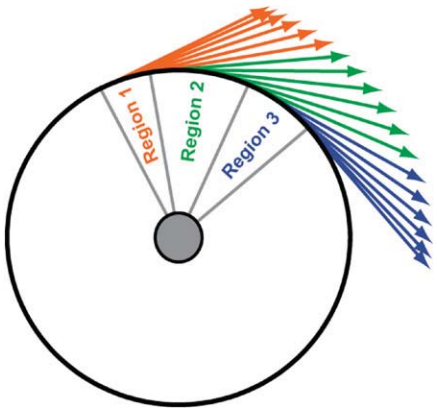

Fig. 8. Tangential force directions during the three regions defined in the push phase. Light grey (Orange), grey (green) and black (blue) arrows represent tangential force vectors in Regions 1, 2 and 3, respectively. (For interpretation of the references to color in this figure legend, the reader is referred to the web version of this article.)

There were some differences in muscle activity between this study and those previously reported. While average and peak ADELT stresses were similar to previous findings, this muscle was not active during the initial region of the push phase (region 1, Fig. 6). PECM activity also occurred later in the push phase. These results are different from previous EMG studies that show high PECM and ADELT activity during early push (e.g., Mulroy et al., 2004; Mulroy et al., 2005). However, both muscles had excitation pattern timing constrained to match the EMG of our wheelchair user, who did not show high activity for either muscle during early push. SUBSC was active over the entire push phase. Although unusual in paraplegic wheelchair users, prolonged SUBSC activity is observed in tetraplegic wheelchair users, which suggests that this is a potentially viable method to provide muscle power during propulsion. Average and peak SUPSP stresses were also low compared to some studies (e.g., Veeger et al., 2002), but were similar to muscle intensity values reported by Mulroy et al. (2005).

The analysis showed that most muscles exert forces in both the tangential and radial directions simultaneously at some point during the push (Figs. 6 and 7), suggesting that pushing along a circular path is not optimal for converting muscle force into a tangential handrim force. This inefficiency is highlighted by the changes in BIC and TRI that occur across FEF conditions. In the nominal simulation, the BIC group contributes to the tangential force early in the push phase followed by contributions by the TRI group (Fig. 6). However, both these groups exert a radial force that is similar in magnitude to their tangential force contributions (Fig. 7). This may explain why TRI is used less in the maximal FEF simulation, instead being replaced by shoulder muscles (i.e. PECM and INFSP) that generate greater tangential and less radial force (Figs. 6 and 7). The decreased use of the elbow extensors and increased use of rotator cuff muscles are consistent with the findings of Bregman et al. (2008), who found that the elbow joint moment changed from having a peak extensor moment to a

peak flexor moment when increasing FEF. This result is also consistent with the suggestion by Veeger (1999) and supported by the study of de Groot et al. (2002b) that force generation must switch from muscles spanning the elbow to those that cross the shoulder to produce a more effective force, which may result in an overall increase in muscle activity and higher metabolic cost. The analysis of the average and peak muscle stresses performed in our study indeed showed that most of the increases occurred in shoulder muscles when maximizing FEF (Fig. 5).

During the push phase, the direction of the tangential force constantly changes as the hand follows the handrim (Fig. 8). When the tangential force has an upward component (region 1, Fig. 8), the reaction force moves the humerus inferiorly, which may reduce the need for rotator cuff muscle activity to stabilize the joint. This reaction force is then systematically redirected downward as the hand moves forward, resulting in a superiorly directed shoulder force at the end of the push, which has been associated with shoulder pathologies (Mercer et al., 2006). As a result, increasing the tangential force during the end of the push phase may increase the likelihood of shoulder injury by amplifying the superiorly directed shoulder force. The maximal FEF simulation increased FEF mainly during regions 2 and 3, which suggests that encouraging wheelchair users to increase FEF will likely increase the superior shoulder force over much of the push and the likelihood of sustaining a shoulder injury.

Wheelchair propulsion is similar to pedaling a bicycle in that the motion is constrained to follow a circular path. Previous pedaling studies have shown that increasing pedal force effectiveness reduces the maximal power output (Doorenbosch et al., 1997) and gross efficiency (Korff et al., 2007). These results and those analyzing wheelchair propulsion suggest that increasing FEF does not reduce neuromuscular demand. Instead, there appears to be a balance between satisfying the competing demands of increasing effective force to meet wheelchair propulsion requirements and reducing total UE demand.

A potential limitation of this study was that the wrist joint was fixed in the model. Previous studies have shown that the hand can apply a pure moment about the wheel axis (e.g., Veeger, 1999), which is usually associated with wrist movement and has the potential to influence muscle force requirements during the push phase. Veeger (1999) investigated the potential consequences of removing the hand moment and found an increase in elbow extensor muscle requirements. However, the present study used a consistent model between the different conditions to investigate relative changes in muscle demand. As a result, differences between FEF values would likely be similar when using a model with a wrist joint. In addition, previous studies have shown that peak and average wrist joint moments during propulsion are much lower than those at the elbow and shoulder joints (e.g., Robertson et al., 1996; Sabick et al., 2004). Thus, the influence of using a fixed wrist on the study results is expected to be minimal.

In summary, there appears to be an optimal FEF value that minimizes UE demand. Maximizing FEF resulted in higher muscle stress and total muscle work. Muscle use also shifted from the elbow to the shoulder, which adds to the already high demands placed on these muscles. Minimizing FEF also increased total muscle work due to an increased need for higher muscle forces, resulting in more muscle co-contraction. Therefore, the optimal FEF value appears to represent a balance between increasing push force effectiveness to increase mechanical efficiency and minimizing overall UE demand. While likely to be similar among users, the specific optimal value will be unique to each individual due to differences in push mechanics and neuromusculoskeletal systems. Thus, care should be taken in using FEF as a metric to reduce UE demand.

Conflict of interest statement

There is no conflict of interest regarding the publication of this manuscript.

Acknowledgement

This work was supported by NIH grant R01 HD053732.

References

Aissaoui, R., Arabi, H., Lacoste, M., Zalzal, V., Dansereau, J., 2002. Biomechanics of manual wheelchair propulsion in elderly: system tilt and back recline angles. American Journal of Physical Medicine and Rehabilitation 81, 94–100.

Ambrosio, F., Boninger, M.L., Souza, A.L., Fitzgerald, S.G., Koontz, A.M., Cooper, R.A., 2005. Biomechanics and strength of manual wheelchair users. The Journal of Spinal Cord Medicine 28, 407–414.

Boninger, M.L., Cooper, R.A., Baldwin, M.A., Shimada, S.D., Koontz, A., 1999. Wheelchair pushrim kinetics: body weight and median nerve function. Archives of Physical Medicine and Rehabilitation 80, 910–915.

Boninger, M.L., Cooper, R.A., Robertson, R.N., Shimada, S.D., 1997. Three-dimensional pushrim forces during two speeds of wheelchair propulsion. American Journal of Physical Medicine and Rehabilitation 76, 420–426.

Boninger, M.L., Souza, A.L., Cooper, R.A., Fitzgerald, S.G., Koontz, A.M., Fay, B.T., 2002. Propulsion patterns and pushrim biomechanics in manual wheelchair propulsion. Archives of Physical Medicine and Rehabilitation 83, 718–723.

Bregman, D.J., Drongelen, S.V., Veeger, H.E., 2008. Is effective force application in handrim wheelchair propulsion also efficient? Clinical Biomechanics 24, 13–19.

Clauser, C.E., McConville, J.T., Young, J.W., 1969. Weight, Volume, and Center of Mass of Segments of the Human Body. Wright–Patterson Air Force Base, Dayton, OH.

Dallmeijer, A.J., van der Woude, L.H., Veeger, H.E., Hollander, A.P., 1998. Effectiveness of force application in manual wheelchair propulsion in persons with spinal cord injuries. American Journal of Physical Medicine and Rehabilitation 77, 213–221.

Davy, D.T., Audu, M.L., 1987. A dynamic optimization technique for predicting muscle forces in the swing phase of gait. Journal of Biomechanics 20, 187–201.

de Groot, J.H., Brand, R., 2001. A three-dimensional regression model of the shoulder rhythm. Clinical Biomechanics 16, 735–743.

de Groot, S., Veeger, D.H., Hollander, A.P., Van der Woude, L.H., 2002a. Wheelchair propulsion technique and mechanical efficiency after 3 weeks of practice. Medicine and Science in Sports and Exercise 34, 756–766.

de Groot, S., Veeger, H.E., Hollander, A.P., van der Woude, L.H., 2002b. Consequence of feedback-based learning of an effective hand rim wheelchair force production on mechanical efficiency. Clinical Biomechanics 17, 219–226.

de Groot, S., Veeger, H.E., Hollander, A.P., van der Woude, L.H., 2004. Effect of wheelchair stroke pattern on mechanical efficiency. American Journal of Physical Medicine and Rehabilitation 83, 640–649.

Desroches, G., Aissaoui, R., Bourbonnais, D., 2008a. The effect of resultant force at the pushrim on shoulder kinetics during manual wheelchair propulsion: a simulation study. IEEE Transactions on Biomedical Engineering 55, 1423–1431.

Desroches, G., Aissaoui, R., Bourbonnais, D., 2008b. Relationship between resultant force at the pushrim and the net shoulder joint moments during manual wheelchair propulsion in elderly persons. Archives of Physical Medicine and Rehabilitation 89, 1155–1161.

Doorenbosch, C.A., Veeger, D.H., van Zandwijk, J.P., van Ingen Schenau, G.J., 1997. On the effectiveness of force application in guided leg movements. Journal of Motor Behavior 29, 27–34.

Finley, M.A., Rasch, E.K., Keyser, R.E., Rodgers, M.M., 2004. The biomechanics of wheelchair propulsion in individuals with and without upper-limb impairment. Journal of Rehabilitation Research and Development 41, 385–394.

Finley, M.A., Rodgers, M.M., 2004. Prevalence and identification of shoulder pathology in athletic and nonathletic wheelchair users with shoulder pain: A pilot study. Journal of Rehabilitation Research and Development 41, 395–402.

Goffe, W.L., Ferrier, G.D., Rogers, J., 1994. Global optimization of statistical functions with simulated annealing. Journal of Econometrics 60, 65–99.

Goosey-Tolfrey, V.L., Lenton, J.P., Fowler, N., van der woude, L., Nicholson, G., Batterham, A., 2006. The influence of push frequency on force application during steady-state hand-rim wheelchair propulsion. Medicine and Science in Sports and Exercise 38, S395–S396.

Guo, L.Y., Su, F.C., An, K.N., 2006. Effect of handrim diameter on manual wheelchair propulsion: mechanical energy and power flow analysis. Clinical Biomechanics 21, 107–115.

Happee, R., Van der Helm, F.C., 1995. The control of shoulder muscles during goal directed movements, an inverse dynamic analysis. Journal of Biomechanics 28, 1179–1191.

Holzbaur, K.R., Murray, W.M., Delp, S.L., 2005. A model of the upper extremity for simulating musculoskeletal surgery and analyzing neuromuscular control. Annals of Biomedical Engineering 33, 829–840.

Korff, T., Romer, L.M., Mayhew, I., Martin, J.C., 2007. Effect of pedaling technique on mechanical effectiveness and efficiency in cyclists. Medicine and Science in Sports and Exercise 39, 991–995.

Kotajarvi, B.R., Basford, J.R., An, K.N., Morrow, D.A., Kaufman, K.R., 2006. The effect of visual biofeedback on the propulsion effectiveness of experienced wheelchair users. Archives of Physical Medicine and Rehabilitation 87, 510–515.

Lin, C.J., Lin, P.C., Su, F.C., An, K.N., 2009. Biomechanics of wheelchair propulsion. Journal of Mechanics in Medicine and Biology 9, 229–242.

Lin, H.T., Su, F.C., Wu, H.W., An, K.N., 2004. Muscle forces analysis in the shoulder mechanism during wheelchair propulsion. Proceedings of the Institution of Mechanical Engineers Part H-Journal of Engineering in Medicine 218, 213–221.

Menegaldo, L.L., de Toledo Fleury, A., Weber, H.I., 2004. Moment arms and musculotendon lengths estimation for a three-dimensional lower-limb model. Journal of Biomechanics 37, 1447–1453.

Mercer, J.L., Boninger, M., Koontz, A., Ren, D., Dyson-Hudson, T., Cooper, R., 2006. Shoulder joint kinetics and pathology in manual wheelchair users. Clinical Biomechanics 21, 781–789.

Mulroy, S.J., Farrokhi, S., Newsam, C.J., Perry, J., 2004. Effects of spinal cord injury level on the activity of shoulder muscles during wheelchair propulsion: an electromyographic study. Archives of Physical Medicine and Rehabilitation 85, 925–934.

Mulroy, S.J., Newsam, C.J., Gutierrez, D.D., Requejo, P., Gronley, J.K., Haubert, L.L., Perry, J., 2005. Effect of fore-aft seat position on shoulder demands during wheelchair propulsion: part 1. A kinetic analysis. The Journal of Spinal Cord Medicine 28, 214–221.

Neptune, R.R., Kautz, S.A., Zajac, F.E., 2001. Contributions of the individual ankle plantar flexors to support, forward progression and swing initiation during walking. Journal of Biomechanics 34, 1387–1398.

Price, R., Ashwell, Z.R., Chang, M.W., Boninger, M.L., Koontz, A.M., Sisto, S.A., 2007. Upper-limb joint power and its distribution in spinal cord injured wheelchair users: steady-state self-selected speed versus maximal acceleration trials. Archives of Physical Medicine and Rehabilitation 88, 456–463.

Raasch, C.C., Zajac, F.E., Ma, B., Levine, W.S., 1997. Muscle coordination of maximum-speed pedaling. Journal of Biomechanics 30, 595–602.

Richter, W.M., Axelson, P.W., 2005. Low-impact wheelchair propulsion: achievable and acceptable. Journal of Rehabilitation Research and Development 42, 21–33.

Robertson, R.N., Boninger, M.L., Cooper, R.A., Shimada, S.D., 1996. Pushrim forces and joint kinetics during wheelchair propulsion. Archives of Physical Medicine and Rehabilitation 77, 856–864.

Rozendaal, L.A., Veeger, H.E., van der Woude, L.H., 2003. The push force pattern in manual wheelchair propulsion as a balance between cost and effect. Journal of Biomechanics 36, 239–247.

Sabick, M.B., Kotajarvi, B.R., An, K.N., 2004. A new method to quantify demand on the upper extremity during manual wheelchair propulsion. Archives of Physical Medicine and Rehabilitation 85, 1151–1159.

van Drongelen, S., van der Woude, L.H., Janssen, T.W., Angenot, E.L., Chadwick, E.K., Veeger, D.H., 2005. Glenohumeral contact forces and muscle forces evaluated in wheelchair-related activities of daily living in able-bodied subjects versus subjects with paraplegia and tetraplegia. Archives of Physical Medicine and Rehabilitation 86, 1434–1440.

Veeger, H.E., 1999. Biomechanics of manual wheelchair propulsion. In: Van der Woude, L.H., Hopman, M.T., Kemenade, C.H. (Eds.), Biomedical Aspects of Manual Wheelchair Propulsion: The State of the Art II. IOS Press, Amsterdam, The Netherlands, pp. 86–95.

Veeger, H.E., Hadj Yahmed, M., van der Woude, L.H., Charpentier, P., 1991. Peak oxygen uptake and maximal power output of Olympic wheelchair-dependent athletes. Medicine and Science in Sports and Exercise 23, 1201–1209.

Veeger, H.E., Rozendaal, L.A., van der Helm, F.C., 2002. Load on the shoulder in low intensity wheelchair propulsion. Clinical Biomechanics 17, 211–218.

Winters, J.M., Stark, L., 1988. Estimated mechanical properties of synergistic muscles involved in movements of a variety of human joints. Journal of Biomechanics 21, 1027–1041.

Zajac, F.E., 1989. Muscle and tendon: properties, models, scaling, and application to biomechanics and motor control. Critical Reviews in Biomedical Engineering 17, 359–411.